The Evolution of Neogene Terrestrial Ecosystems in Europe

Edited by

JORGE AGUSTI

LORENZO ROOK

and

PETER ANDREWS

3 Pliocene tephra correlations between East African hominid localities, the Gulf of Aden, and the Arabian Sea

Peter B. deMenocal and Francis H. Brown

Introduction

The Pliocene–Pleistocene chronology of hominid and other vertebrate evolution in East Africa is largely constrained by isotopic dating and regional intercorrelation of volcanic ash layers. Some eruptions were of sufficient magnitude or duration that their widespread tephra dispersal defines a series of dated marker horizons throughout the fossil-bearing sedimentary deposits of Tanzania, Uganda, Kenya, and Ethiopia (Brown, 1982; Feibel et al., 1989; Haileab & Brown, 1992, 1994; Pickford et al., 1991; WoldeGabriel et al., 1994). Although many of the larger eruptive events have been dated directly the ages of many tephra are only constrained by indirect stratigraphic interpolation between dated levels. The geochemical compositions of volcanic glasses from each eruption are unique, providing a definitive means to establish broad tephrostratigraphic correlations linking the regional climatic, tectonic, and biologic histories of this distinctive archive of Earth history.

This same tephrostratigraphic approach has been used to extend the East African tephra correlations into the continuous and well-dated marine sediment record of regional and global paleoclimate variability (Brown et al., 1992; Sarna-Wojcicki et al., 1985). These authors identified several megascopic volcanic ash layers within Deep-Sea Drilling Project (DSDP) sites from the Gulf of Aden, nearly 1000 km northeast of hominid localities in Ethiopia and Kenya. Major element chemistries of volcanic glass shards extracted from these marine sediments were used to establish precise tephrostratigraphic correlations into the fossil-bearing East African sedimentary sequences. Moreover, controversy concerning the ages of specific eruptive events which then defined key temporal junctures in early hominid evolution could be tested using the independent marine sediment chronostratigraphic framework (Brown et al., 1992; Sarna-Wojcicki et al., 1985). A more comprehensive effort to establish more Pliocene–Pleistocene tephra correlations between terrestrial and marine sequences was hampered by incomplete and often disturbed core recovery at these early DSDP sites in the Gulf of Aden.

Subsequent advances in deep-sea drilling technology and the return of scientific ocean drilling to the Arabian Sea present a new opportunity to establish tephrostratigraphic links between East African terrestrial and adjacent marine sedimentary sequences. Leg 117 of the Ocean Drilling Program drilled twelve sites off the Omani margin and Arabian Sea (Fig. 3.1;

24
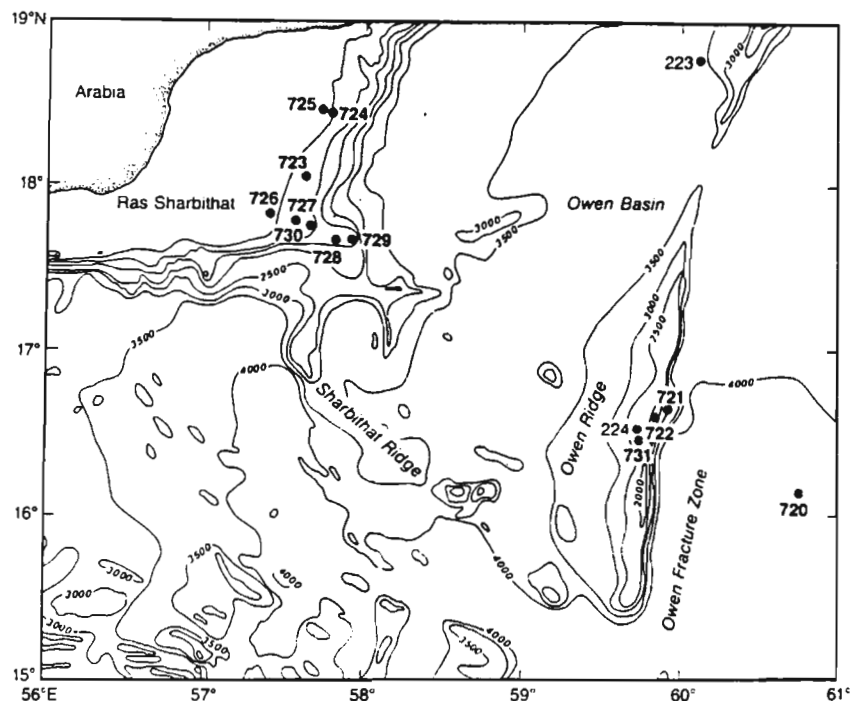
[Figure 3.1]
Locations of Ocean Drilling Program (ODP) drill sites in the Arabian Sea.

Prell & Niitsuma, 1988; Prell *et al.*, 1988) in an effort to reconstruct the late Cenozoic history of the Asian monsoon and associated Arabian Sea upwelling. Coring of Pliocene–Pleistocene sediments was accomplished using an advanced hydraulic piston coring system which recovered complete and undisturbed sediments. In a marked improvement over earlier drilling efforts in the Gulf of Aden multiple holes were drilled at each site permitting the construction of complete, composite sedimentary sequences extending to the latest Miocene (deMenocal & Bloemendal, 1995; deMenocal *et al.*, 1991; Murray & Prell, 1991). Subsequent study of Sites 721 and 722 from the Arabian Sea has produced long and continuous orbitally tuned time series of Pliocene–Pleistocene variations in regional aridity (Clemens & Prell, 1990, 1991; deMenocal, 1995; deMenocal & Bloemendal, 1995) and the strength of the Asian monsoon (Clemens & Prell, 1990, 1991; Clemens *et al.*, 1996; Prell & Kutzbach, 1992). Although these sites are some 2000 km distant from East African source volcanoes, numerous discrete levels with enhanced ash shard abundances have been identified which are temporally correlative with known East African tephra layers (deMenocal & Bloemendal, 1995). The present study provides a comprehensive survey of tephra-

bearing levels within the Pliocene–Pleistocene sediments at Sites 721 and
722.

Research strategy

The Site 721 and 722 sediments present an unique opportunity to place the
East African sedimentary sequences, and the fossils they contain, within the
context of the continuous and very detailed marine paleoclimatic record
and chronostratigraphic framework. The research strategy is to use the
oxide compositional signatures of volcanic glass shards extracted from Sites
721 and 722 to define these terrestrial–marine correlations. We employ a
similar approach to that described by Sarna-Wojcicki & Davis (1991) which
correlates tephra using glass chemistry, with confirmation by sequence (i.e.,
the known temporal succession of eruptions). The challenge is that ash
shards are extremely rare in these Site 721 and 722 sediments which are so
distant from East African source volcanoes. However, once firmly estab-
lished these tephrostratigraphic linkages present several new research op-
portunities. The correlations provide a direct way to compare the radioiso-
topic ages of East African tuffs with the orbitally tuned ages derived for the
marine sediment record (e.g. McDougall et al., 1992; Renne et al., 1993;
Walter, 1994). Additionally, the correlations link specific East African fluvio-
lacustrine stratigraphic sections to the marine paleoclimatic and
paleoceanographic records, providing a direct means to assess past climatic
linkages between the two regions. Finally, a full suite of tephra correlations
will provide the means to directly test hypotheses linking Pliocene–Pleis-
tocene changes in hominid and other African vertebrate evolution to re-
gional changes in climate (Behrensmeyer et al., 1997; deMenocal, 1995;
Grine, 1986; Vrba, 1985, 1995). In this paper we present electron microprobe
major element oxide data for five tephra horizons at Sites 721 and 722
between 4.0 and 3.5 Ma, and establish correlations to East African tuffs and
Gulf of Aden tephra. Approximately 25 tephra-rich layers can be analysed
within the Pliocene–Pleistocene interval at Sites 721 and 722.

Site locations and regional climatology

Sites 721 (16° 40.6'N, 59° 51.9'E, 1944 m) and 722 (16° 37.3'N, 59° 47.7'E,
2028 m) were both drilled near the crest of the Owen Ridge in the Arabian
Sea (Fig. 3.1), separated by approximately 20 km. The ridge setting was
selected specifically to recover records of pelagic sedimentation in the

26 Arabian Sea to record past variations in regional climate and surface ocean changes associated with the late Cenozoic evolution of the Indian monsoon. The relative shallowness of these sites places them above the calcite lysocline and precludes any significant contribution from downslope processes associated with the Indus fan. Pliocene–Pleistocene sedimentation rates average ~ 3–4 cm/kyr based on preliminary biostratigraphic age control (Prell & Niitsuma, 1988) and sediments are predominantly composed of nannofossil ooze with varying concentrations of terrigenous clay and silt.

Monsoonal circulation, such as that associated with the African, Indian, and Southeast Asian monsoonal regions, results as a consequence of the differing heat capacities of land and water. Sensible heating warms land surfaces much more rapidly than an ocean mixed layer (Hastenrath, 1985). During the winter months the South Asian landmass cools more efficiently than the adjacent North Indian Ocean and a broad high pressure cell develops over Siberia and the Tibetan Plateau. Dry and variable northeast trade winds develop over the southeast Asian region, including the Arabian Sea from October to April (Fig. 3.2a). Sensible heating during the Northern Hemisphere summer promotes the development of a strong low pressure cell over South Asia that establishes very strong regional cyclonic circulation over South Asia from May to September. Strong (15 m/s) moisture-laden southwest winds (Somali Jet) parallel the East African, Arabian, and Omani coasts during the summer, bringing monsoon rains to southern Asia (Fig. 3.2b). As a dynamical response to the surface wind stress field, cool, nutrient-rich waters upwell off Arabia and Oman and support high surface ocean productivity in the Arabian Sea.

Atmospheric sampling, satellite images, and sediment trap studies have demonstrated that wind-borne mineral grains (eolian dust) are entrained from Mesopotamian, Arabian, and northeast African sources during the peak months of the summer monsoon: June, July, and August (Clemens et al., 1996; Nair et al., 1989; Pye, 1987; Sirocko, 1989; Sirocko & Sarnthein, 1989). Sediment trap data from the Arabian Sea indicate that 80% of the annual terrigenous flux to the western Arabian Sea occurs during the summer months (Nair et al., 1989). Geochemical and mineralogic data indicate that the Mesopotamian floodplains are by far the largest source of eolian dust to the Arabian Sea, although minor contributions from East Africa are also indicated (Sirocko, 1989; Sirocko et al., 1996; Sirocko & Sarnthein, 1989). Given their trajectory, strength, and persistence, the summer SW monsoon winds are an efficient vector for transporting East African volcanic ash shards to the Arabian Sea (Fig. 3.2b).
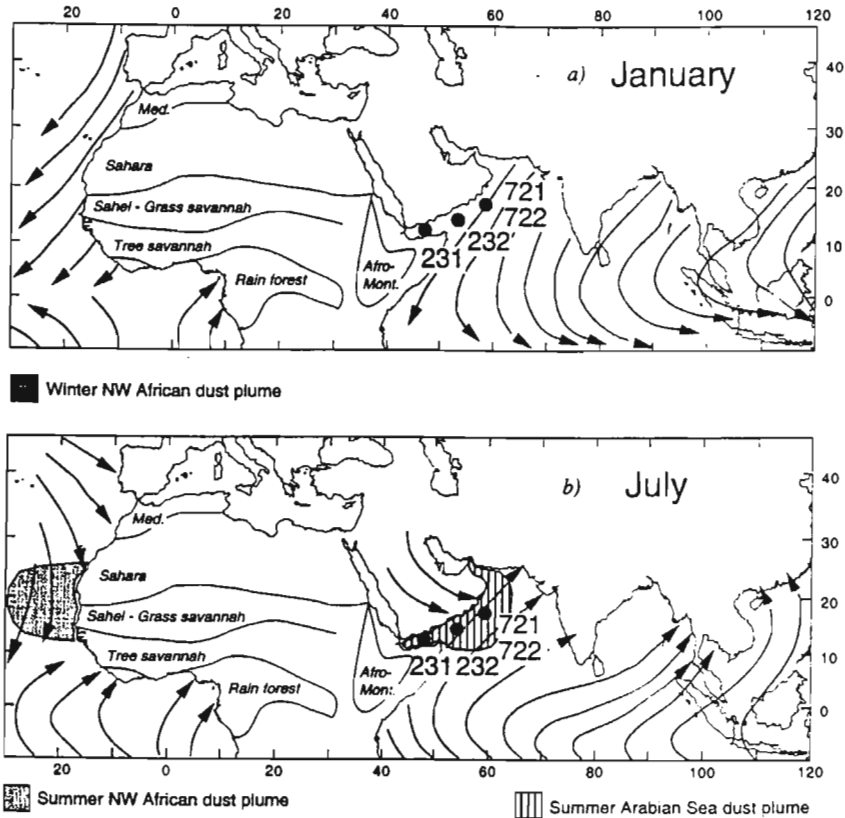
[Figure 3.2]
Boreal winter (a) and summer (b) surface winds over northeast Africa and the Arabian Sea.

Pliocene–Pleistocene variability of regional climate and the Indian monsoon

The sediments of Site 721 and 722 have been the focus of much research into the late Cenozoic evolution of the Indian monsoon and regional climate. Initial work at Site 722 demonstrated that large changes in regional aridity were linked to the Pleistocene succession of glacial–interglacial cycles (Clemens & Prell, 1990, 1991). Eolian dust fluxes to Site 722 during glacial maxima were three to five times higher than observed for interglacial periods; these low-latitude aridity cycles were observed to be directly in-phase with the oxygen isotopic record of high-latitude glacial–interglacial cycles. Parallel analysis of the terrigenous (eolian) grain size variations at Site 722, which monitor variations in the strength of the summer SW monsoon winds, further demonstrated that the Indian monsoon intensity was closely linked to

28

variations in summer insolation resulting from orbital precession (at the 23–19 kyr periodicity). This first-order relation between sensible heating variations (forcing due to orbital variations in seasonal radiation distribution) and the strength of the summer monsoon circulation (the climate response) has been a focus of many atmospheric climate model studies (e.g. Kutzbach, 1981; Kutzbach & Guetter, 1986; Prell & Kutzbach, 1987).

Analysis of the full Pliocene–Pleistocene interval (last *c.* 5 Ma) at Sites 721 and 722 has produced new perspectives on the evolution of regional climate associated with the initial onset and subsequent growth of high-latitude glacial cycles after *c.* 2.8 Ma. Study of eolian dust variations at Sites 721 and 722, as well as analysis of six other sites in the Gulf of Aden and off subtropical West Africa have demonstrated that the onset of large amplitude regional aridity cycles was closely linked to the development of high-latitude glacial cycles (Bloemendal & deMenocal, 1989; Clemens *et al.*, 1996; deMenocal, 1995; deMenocal & Bloemendal, 1995; deMenocal *et al.*, 1991, 1993; Tiedemann *et al.*, 1994). Several features of the Pliocene–Pleistocene evolution of subtropical African aridity variations are common to all of these sites (deMenocal, 1995). Prior to 2.8 Ma subtropical African aridity varied at the 23–19 kyr period associated with low-latitude radiation forcing of monsoonal climate, whereas after 2.8 Ma African aridity followed the longer 41 kyr and then 100 kyr periods associated with glacial–interglacial cycles of the late Pliocene and Pleistocene, documenting the post-2.8 Ma regulation of this low-latitude climate system by high-latitude glacial climates. Distinct shifts in African eolian variability were observed at 2.8 Ma, 1.7 Ma, and 1.0 Ma, each tied to coeval shifts in high-latitude climate. This sensitivity of African climate to high-latitude glacial boundary conditions has been documented using general circulation model experiments (Clemens *et al.*, 1991; deMenocal & Rind, 1993; Kutzbach & Guetter, 1986; Prell & Kutzbach, 1987). Based on analysis of the terrigenous (eolian) grain size record over the last 3.5 Ma at Site 722, Clemens *et al.* (1996) documented discrete shifts in the intensity and phase of the Indian monsoon at 2.6 Ma, 1.7 Ma, and 1.2 Ma, and 0.6 Ma, further emphasizing the importance of high- and low-latitude climate linkages throughout the Pliocene and Pleistocene.

Analytical methods

A primary objective of the present study is to document a continuous Pliocene–Pleistocene history of explosive volcanism in East Africa through the stratigraphic record of tephra deposition in the Arabian Sea. Consequently, we employed a sampling strategy whereby the full Site 721/722

composite sequence spanning the last 4.5 Ma (c. 135 m; see Table 3.1) was continuously scrape sampled across the core diameter at 30 cm intervals using a Teflon spatula, yielding approximately 2–3 g of dry sediment. Using an average Pliocene–Pleistocene sedimentation rate of 3.2 cm/kyr; (Clemens et al., 1996; Murray & Prell, 1991), this sample interval is equivalent to ~ 10 kyr, our nominal temporal resolution in this study.

Samples were freeze-dried, weighed, and then decarbonated using 100 ml 1M acetic acid and placed on a shaker table for one hour. After settling, samples were decanted and washed once with deionized water, and then wet sieved at 38 μm. The > 38 μm fraction was saved, freeze-dried, and weighed. Grain mount slides were prepared for all 380 samples using Permount medium and large area (50 × 25 mm) coverslips. Optically isotropic ash shards were identified and counted to obtain semi-quantitative estimates for shard abundance, which ranged between 0–1800 shards per slide. Tephra-bearing layers were never visibly evident from the split core and shards were generally extremely rare except for six levels where shards were very abundant. Median shard sizes were approximately 40–60 μm which proved to be too small for manual extraction. Shard morphology was dominated by clear, arcuate fragments with the larger shards having well-defined bubble-wall junctions and rare cylindrical vesicles.

Samples with highest shard abundances were further concentrated using a sodium polytungstate (Na_2WO_4) heavy-liquid separation step ($\rho = 2.2$ g/cc) to separate ash shards and other detrital mineral grains ($\rho > 2.5$ g/cc) from lighter but very abundant diatoms and radiolaria ($\rho = 1.9$–2.2 g/cc). Samples were added to a 2.2 g/cc Na_2WO_4 solution, sonicated, then centrifuged for 3 minutes. The basal 1 cm of the centrifuge tube (now containing the shards and other detrital mineral grains) was frozen in liquid nitrogen and remaining supernatant (containing diatoms and radiolaria) was decanted and the tube walls were rinsed with deionized water. After thawing the shard-bearing Na_2WO_4 slurry was then captured and rinsed using a 0.2 μm filter. This technique proved to be very effective in concentrating the shard abundances and removing the biogenic components; the final concentrate typically comprised < 1% of the original dry bulk sediment mass. After drying these samples were then mounted for microprobe analysis.

Samples were analysed on a Cameca SX-50 electron microprobe equipped with four wavelength-dispersive spectrometers. The accelerating voltage was 15 kV, the beam current 25 nA, and the beam diameter between 5 and 25 μm. Elemental concentrations were calculated from relative peak intensities using the $\phi(\rho z)$ algorithm (Pouchou & Pichoir, 1991). The standard for O, Si, Al, and K was natural obsidian. The remaining elements were standardized using minerals and synthetic oxides. In order to assure an

Table 3.1. *Site 721 and 722 composite section*

	Site	Hole	Core	Type	Sect.	Int.	mbsf	adj (m)	mcd
From	722	B	1	H	1	5	0.05	0.00	0.05
To	722	B	1	H	4	50	5.00	0.00	5.00
From	722	A	1	H	3	60	3.60	1.45	5.05
To	722	A	1	H	3	140	4.40	1.45	5.85
From	722	B	2	H	1	30	5.80	0.10	5.90
To	722	B	2	H	6	45	13.45	0.10	13.55
From	722	A	2	H	2	95	12.25	1.35	13.60
To	722	A	2	H	4	35	14.65	1.35	16.00
From	722	B	3	H	1	40	15.50	0.55	16.05
To	722	B	3	H	6	20	22.80	0.55	23.35
From	722	A	3	H	2	65	21.55	1.85	23.40
To	722	A	3	H	4	100	24.90	1.85	26.75
From	722	B	4	H	1	70	25.40	1.40	26.80
To	722	B	4	H	6	90	33.10	1.40	34.50
From	722	A	4	H	3	15	32.15	2.40	34.55
To	722	A	4	H	4	55	34.05	2.40	36.45
From	722	B	5	H	1	65	34.95	1.55	36.50
To	722	B	5	H	7	15	43.45	1.55	45.00
From	722	A	5	H	3	70	42.30	2.75	45.05
To	722	A	5	H	4	125	44.35	2.75	47.10
From	722	B	6	H	1	95	44.85	2.30	47.15
To	722	B	6	H	7	15	53.05	2.30	55.35
From	722	A	6	H	3	75	51.95	3.45	55.40
To	722	A	6	H	7	20	57.40	3.45	60.85
From	721	A	6	H	4	75	53.75	7.15	60.90
To	721	A	6	H	5	45	54.95	7.15	62.10
From	722	A	7	H	1	20	57.70	4.45	62.15
To	722	A	7	H	4	85	62.85	4.45	67.30
From	722	B	8	H	1	50	63.40	3.95	67.35
To	722	B	8	H	6	105	71.45	3.95	75.40
From	722	A	8	H	3	10	70.30	5.15	75.45
To	722	A	8	H	4	105	72.75	5.15	77.90
From	722	B	9	H	1	70	73.20	4.75	77.95
To	722	B	9	H	7	55	82.05	4.75	86.80
From	721	C	10	H	2	5	81.85	5.05	86.90
To	721	C	10	H	2	145	83.25	5.05	88.30
From	722	B	10	H	1	35	83.05	5.30	88.35
To	722	B	10	H	7	35	92.05	5.30	97.35
From	721	C	11	X	3	10	93.00	4.40	97.40
To	721	C	11	X	5	80	96.70	4.40	101.10
From	721	C	12	X	1	50	100.00	1.15	101.15
To	721	C	12	X	4	95	104.95	1.15	106.10
From	722	A	11	X	3	70	99.90	6.25	106.15
To	722	A	11	X	6	135	105.05	6.25	111.30
From	721	C	13	X	1	140	110.50	0.85	111.35
To	721	C	13	X	5	100	116.10	0.85	116.95
From	722	A	12	X	3	10	109.00	8.00	117.00
To	722	A	12	X	5	130	113.20	8.00	121.20

Table 3.1. (*cont*)

	Site	Hole	Core	Type	Sect.	Int.	mbsf	adj (m)	mcd
From	721	C	14	X	2	75	120.95	0.30	121.25
To	721	C	14	X	5	60	125.30	0.30	125.60
From	721	B	14	X	2	135	127.25	− 1.60	125.65
To	721	B	14	X	6	130	133.20	− 1.60	131.60
From	721	C	15	X	3	70	132.00	− 0.35	131.65
To	721	C	15	X	6	130	137.10	− 0.35	136.75

mbsf = meters below seafloor.
adj = depth adjustment in meters required to build composite.
mcd = meters composite depth.

equivalent thickness of the C coating, the obsidian standard and unknowns were coated simultaneously. Details of the analytical method are provided in Nash (1992). Raw elemental percentages were normalized to 100% to remove the effects of variable hydration. Average and standard deviation chemical data for samples from Site 721/722 (Arabian Sea) samples, Site 231/232 (Gulf of Aden), and Turkana Basin tephra are presented in Tables 3.2, 3.3, and 3.4, respectively. The Gulf of Aden chemical data were taken directly from the primary reference (Sarna-Wojcicki *et al.*, 1985), whereas the Turkana Basin chemical data (Table 3.4) were dervied from multiple shard averages of the sample (Brown *et al.*, 1992; Haileab & Brown, 1992, 1994; Sarna-Wojcicki *et al.*, 1985). Original totals (T_o) are given to indicate degree of shard hydration and to permit recalculation to original raw percentages. Analytical standard deviations for SiO_2, TiO_2, Al_2O_3, Fe_2O_3, MnO, MgO, and CaO using our internal standards were 0.5, 0.01, 0.2, 0.03, 0.005, 0.01, and 0.02 weight percent, respectively.

Results

Thirty-nine samples contained sufficient shards for subsequent concentration, presenting between 25 discrete, analytically viable ash layers. Here, we focus on analyses of five tephra-bearing levels between 4.0–3.4 Ma. Several East African tuffs have been dated by K/Ar and [40]Ar/[39]Ar methods within this interval to very high precision (McDougall *et al.*, 1992; Renne *et al.*, 1993; Walter, 1994; Walter & Aronson, 1993). Additionally, many tephra layers within this interval have been correlated between stratigraphic sequences in Kenya and Ethiopia and have been found also within the Gulf of Aden marine sediments. Finally, there exist several tephra horizons within this

Table 3.2. *Electron probe analysis of volcanic glass shards separated from Arabian Sea Sites 721 and 722*

Sample	N	SiO_2	sd	TiO_2	sd	Al_2O_3	sd	Fe_2O_3	sd	MnO	sd	MgO	sd	CaO	sd	Total
722A 11-1 (30-60)	1	76.97	0.50	0.14	0.01	12.74	0.20	1.76	0.03	0.08	0.01	0.06	0.01	0.33	0.02	94.49
721C 13-3 (90-120)	6	76.12	0.58	0.16	0.04	11.48	0.23	2.61	0.07	0.07	0.04	0.03	0.01	0.19	0.01	95.67
722A 12-4 (90-120)	2	76.01	0.06	0.21	0.01	11.11	0.03	2.92	0.14	0.11	0.02	0.01	0.00	0.23	0.00	96.07
722A 11-4 (60-90)	14	75.62	0.37	0.19	0.05	10.99	0.10	3.27	0.06	0.09	0.04	0.04	0.02	0.22	0.05	95.03
722A 11-4 (60-90)	6	75.99	1.34	0.23	0.08	10.42	0.24	4.57	0.20	0.13	0.03	0.03	0.01	0.22	0.01	96.42
722A 12-4 (90-120)	11	75.83	0.88	0.30	0.03	10.57	0.24	4.64	0.13	0.17	0.04	0.03	0.03	0.28	0.06	96.18
722A 11-5 (60-90)	20	74.84	0.29	0.24	0.04	10.22	0.30	4.61	0.47	0.17	0.03	0.02	0.02	0.21	0.02	90.67

Table 3.3. *Electron probe analysis of volcanic glass shards separated from Gulf of Aden Sites 231 and 232 (Sarna-Wojcicki et al., 1985, #1059)*

Sample	N	SiO_2	sd	TiO_2	sd	Al_2O_3	sd	Fe_2O_3	sd	MnO	sd	MgO	sd	CaO	sd	Total
231-19-2 (33-34)	30	76.43	0.6	0.14	0.01	12.50	0.23	1.57	0.06	0.31	0.06	0.05	0.01	0.31	0.06	94.31
231-21-2-(15-17)	15	76.87	0.68	0.13	0.02	11.44	0.24	2.42	0.06	0.18	0.01	0.07	0.01	0.18	0.01	93.20
231-22-1-(82-85)	15	76.68	0.54	0.19	0.03	11.28	0.25	2.73	0.06	0.21	0.01	0.08	0.01	0.21	0.01	92.94
232A-1-4 (42-450	14	75.73	0.66	0.20	0.05	10.61	0.57	3.97	0.18	0.19	0.02	0.16	0.02	0.19	0.02	92.89
231-20-2 (25-28)	15	76.65	0.66	0.23	0.03	10.62	0.35	4.06	0.35	0.19	0.02	0.16	0.02	0.19	0.02	92.48
232A-1-5 (25-27)	15	75.39	0.79	0.24	0.04	10.53	0.45	4.14	0.37	0.19	0.02	0.16	0.02	0.19	0.02	92.68

Table 3.4. *Electron probe analysis of volcanic glass shards separated from Turkana Basin tuffs*

Sample	N	SiO$_2$	sd	TiO$_2$	sd	Al$_2$O$_3$	sd	Fe$_2$O$_3$	sd	MnO	sd	MgO	sd	CaO	sd	Total
82-869	5	76.80	0.21	0.16	0.06	12.73	0.10	1.69	0.06	0.05	0.01	0.06	0.01	0.30	0.02	93.09
K81-485	27	77.91	0.43	0.14	0.02	11.42	0.26	2.48	0.06	0.08	0.03	0.03	0.02	0.20	0.02	92.49
81-602	15	77.03	0.55	0.16	0.04	11.19	0.22	2.81	0.06	0.10	0.02	0.00	0.00	0.22	0.01	93.79
80-295	15	77.43	0.80	0.18	0.04	11.12	0.19	3.19	0.10	0.11	0.01	0.03	0.02	0.19	0.02	91.45
80-295	11	77.33	0.61	0.21	0.05	10.41	0.23	4.43	0.06	0.15	0.03	0.02	0.01	0.20	0.02	90 60
83-1ANU	20	74.48	0.62	0.33	0.06	11.11	0.21	4.56	0.33	0.17	0.03	0.00	0.02	0.30	0.02	95.31
82-742	11	77.85	0.68	0.25	0.03	10.62	0.24	4.62	0.12	0.19	0.02	0.02	0.01	0.21	0.03	95.48

interval that have not been dated directly and reported ages of these key marker horizons are only constrained by stratigraphic interpolation. Thus, the several tephra layers within this interval provide an excellent opportunity to test the tephrostratigraphic and chronologic precision of these terrestrial–marine correlations.

Tephra abundances and the Site 721/722 age model

The volcanic ash shard abundance record from the Site 721/722 composite sequence spanning 0.5–4.5 Ma is shown in Fig. 3.3. Also shown in this figure is the eolian dust record (from these same sites) presented in deMenocal (1995). The temporal sampling resolution of the 721/722 eolian record is 1.5 kyr. We identify approximately 25 discrete ash layers (where shard abundances exceeded 20 shards per slide to maximum values reaching ~ 2000 shards per slide) between 0.5–4.5 Ma. There were many additional levels where ash shards were present (5–20 shards/slide) but these concentrations were judged from experience to be too low to recover sufficient material for analysis.

Focusing on the 4.5–3.0 Ma interval (90–140 mcd) we find approximately 11 discrete ash layers (Fig. 3.4). We can estimate the ages of these ash layers by referring to the orbitally tuned timescale previously developed for this site (deMenocal, 1995; deMenocal & Bloemendal, 1995) (Fig. 3.5). As a brief review, Site 721/722 eolian dust percentages were phase-locked to an orbital composite target signal comprised of 0.66 weighting of orbital precession and 0.34 weighting of orbital obliquity, both of which were aligned for maxima in boreal summer insolation (deMenocal, 1995; deMenocal & Bloemendal, 1995). The rationale for this approach was that early Pliocene dust and upwelling indices suggested that maxima in eolian dust and upwelling indices appeared to be indicating maxima in summer monsoon intensity which climate models indicate should coincide with orbital precession index ($e\sin(\omega)$) minima, and orbital tilt index maxima (Berger & Loutre, 1991; deMenocal, 1995). The Site 721/722 eolian time series is shown adjacent to the orbital insolation tuning target for the 3.0–4.5 Ma interval in Fig. 3.5. Note the very close correspondence (correspondingly high coherency) between the relative amplitude variations of the orbital forcing and paleoclimate (aridity) response for this interval.

As shown by Clemens et al. (1996) the phase of the Indian monsoon response to insolation forcing appears to have been non-stationary over the Pliocene–Pleistocene interval, showing clear phase jumps with respect to a 'phase-stationary' orbital target. These phase jumps require that either high-latitude glacial ice volume and/or the low-latitude monsoon shifted in

Arabian Sea Dust and Volcanic Ash Abundances
0.5 - 4.5 Ma
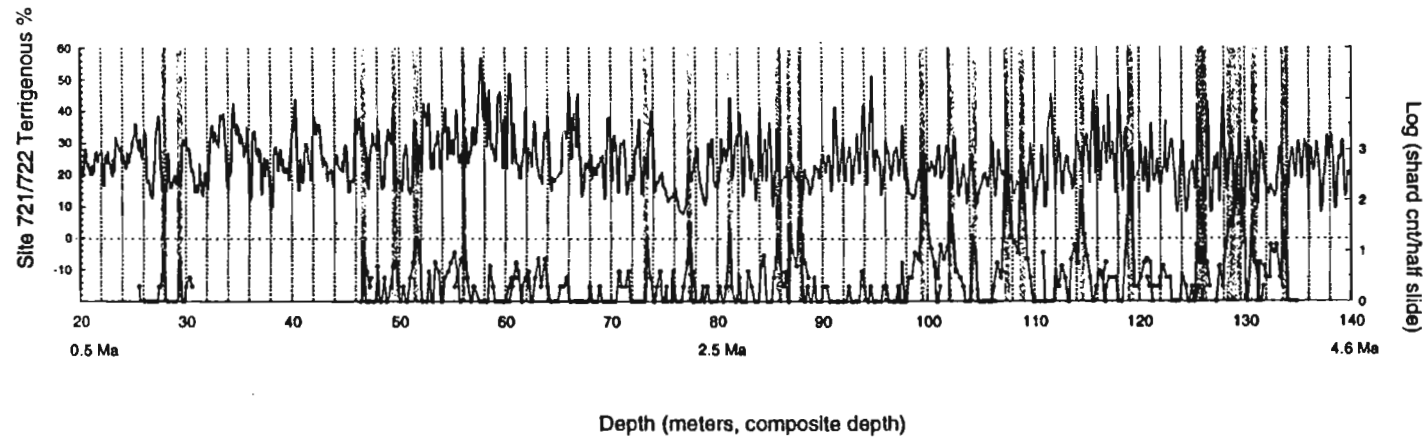
[Figure 3.3]
Volcanic ash shard abundance record derived for the Site 721/722 composite sedimentary sequence between 0.5–4.5 Ma shown adjacent to the Site 721/722 eolian dust record (deMenocal, 1995). Approximately 25 discrete tephra-rich ash layers are identified for this 0.5–4.5 Ma interval. Depths are in meters, composite depth (mcd) based on the composite table shown in Table 3.1. The interval between 30 and 46 mcd (c. 0.8–1.2 Ma) was not sampled in this study.

Arabian Sea Dust and Volcanic Ash Shard Concentrations
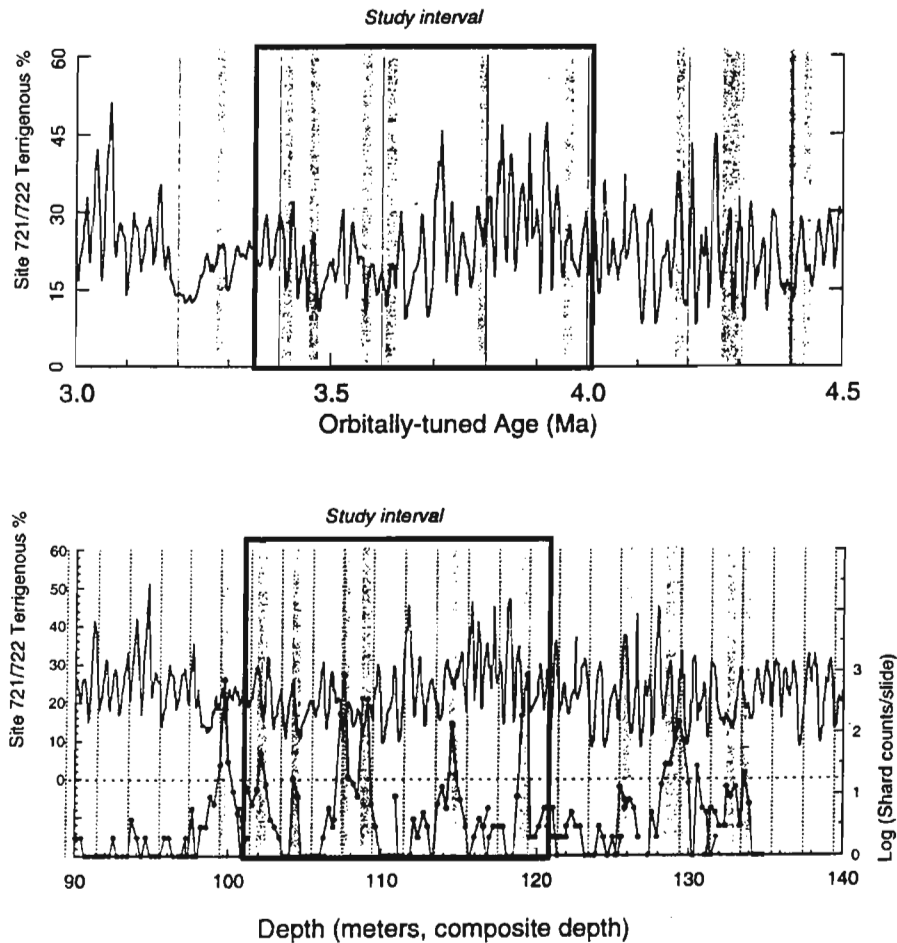
[Figure 3.4]
Volcanic ash abundances and eolian dust percentage at Sites 721/722 for the 3.0–4.5 Ma interval. The eolian timeseries shown was derived from the originally published orbitally tuned timescale (deMenocal, 1995; deMenocal & Bloemendal, 1995). Details of the orbital tuning precision for this interval are shown in Fig. 3.5.

their phase response relative to orbital radiation forcing by c. 5–15 kyr at key times (2.6 Ma, 1.7 Ma, and 1.2 Ma, and 0.6 Ma,) during the Pliocene–Pleistocene. This means that the absolute oxygen isotopic chronology may have a time-varying offset of 5–15 kyr with respect to sideral time, an unresolved problem which potentially applies to our timeseries as well. This offset is small with respect to our chronostratigraphic resolution issues here;

[Figure 3.5]
The orbitally tuned timescale developed for the Site 721/722 eolian timeseries for the 3.0–4.5 Ma interval (deMenocal, 1995; deMenocal & Bloemendal, 1995). Note the close match between the relative amplitudes of the orbital radiation forcing target (Berger & Loutre, 1991) and the eolian (aridity) paleoclimate response over this interval. Although the precision of the tuning process is ± 5 kyr, remaining uncertainty surrounding the precise phase of the monsoon response to insolation forcing (Clemens et al., 1996) introduces an additional uncertainty of 5–15 kyr.

Orbitally-Tuned Chronology

Berger & Loutre (1991)
Orbital Composite
2P+1T

Site 721/722 Terrigenous %

0   15   30   45   60

3.0

Orbitally-tuned
Age (Ma)

3.5

4.0

4.5

Inc. Summer
Insolation ⟶

Analyzed in
this study ★
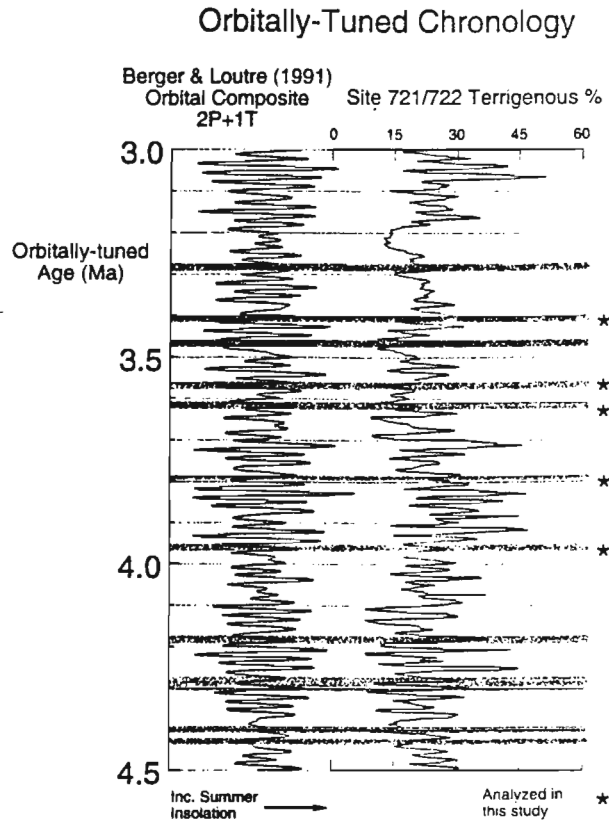
however, there are larger paleoclimatic and paleoceanographic implications (Clemens et al., 1996).

Chemical correlation results of selected tephra layers between 3.4–4.0 Ma

Five tephra-bearing samples from the 3.4–4.0 Ma interval at Sites 721 and 722 were selected for subsequent concentration, mounting, and analysis by electron microprobe. Between six and twenty shards were analysed per sample with several determinations per shard. Averaged chemical data (normalized to 100% to correct for variable hydration), standard deviations, and original totals (T_0) for these samples are listed in Table 3.2. Oxide crossplots for these five Arabian Sea samples are shown in Figs. 3.6–3.10 along with oxide data from Turkana Basin tuffs and analyses on extracted Gulf of Aden tephra (Brown et al., 1992; Sarna-Wojcicki et al., 1985).

We use the Similarity Coefficient (SC) as a means to quantify the chemi-

Table 3.5. *Similarity Coefficients between Site 721/722, Turkana Basin, and Site 231/2 tephra chemistries (5-elements)*

Sample	SC	WRT tuff . . .	Tuff Name	SC	WRT Sites 231/2 . . .
722A 11-1 (30-60)	0.95	82-869	β Tulu Bor	0.96	231 19-2 (33-34)
721C 13-3 (90-120)	0.95	K81-485	Wargolo	0.92	231 21-2 (15-17)
722A 12-4 (90-120)	0.92	83-1ANU	Moiti, lo-Fe	0.94	231 22-1 (82-85)
722A 11-4 (60-90)	0.95	80-295	Lokochot, lo-Fe		
722A 11-4 (60-90)	0.95	80-295	Lokochot, hi-Fe	0.94	231 20-2 (25-28)
722A 12-4 (90-120)	0.95	81-602	Moiti, hi-Fe		
722A 11-5 (60-90)	0.98	82-742	Lomogol	0.95	232A 1-5 (25-27)

cal similarity between an analysed tephra and other candidate tephra matches (Borchardt *et al.*, 1972). The SC is computed as:

$$SC = 1/n \cdot \Sigma \, | \, (x_n - x_0) \, |$$

where x_n and x_0 are the separate oxide compositions for the sample tephra and the comparison target tephra, and oxide differences are summed for n-oxides (five oxides in our case). We computed SC values using the following five oxides: SiO_2, TiO_2, Al_2O_3, Fe_2O_3, and CaO (Brown *et al.*, 1992; Sarna-Wojcicki *et al.*, 1985). The SC statistic equals unity for samples with identical chemical compositions. In practice the SC values can range between 1.00–0.97 for replicate analyses whose compositions are within one standard deviation of the mean composition. In all cases, the tuff correlations discussed below represented the best compositional match to the specified East African tuff.

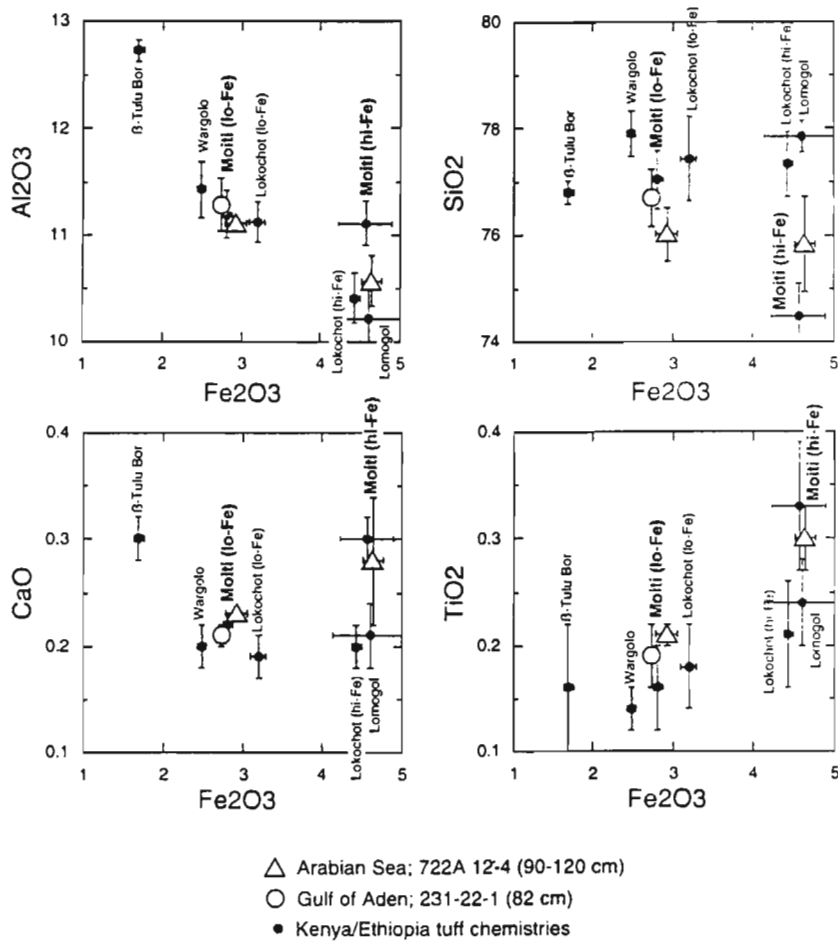*Sample 722A 12-4 (90–120 cm) – Moiti Tuff (SC = 0.92 and 0.95)*

The five oxide bivariate plots for sample 722A 12-4 (90–120 cm) are shown in Fig. 3.6, and these data are compared to published oxide compositions for other East African tuffs of this approximate age range, including the Moiti, Wargolo, Lomogol, Lokochot, and β-Tulu Bor Tuffs (Brown, 1982; Brown *et al.*, 1992; Sarna-Wojcicki *et al.*, 1985). We found that shards within this sample fell into bimodal high-Fe ($n = 11$) and low-Fe ($n = 2$) compositions. The Moiti Tuff was the only tuff in this age range (*c.* 4.0 Ma) which had this dual low-Fe (K81-602, Turkana Basin) and high-Fe (83-1 ANU, Turkana Basin) composition (Tables 3.2–3.4) and closely matched our sample for all five oxides. The computed SC values for the low- and high-Fe Moiti compositions were 0.95 and 0.92, respectively (Table 3.5, Fig. 3.6). Only two shards were analysed for the low-Fe Moiti tephra within 722A 12-4 (90–120 cm) and this may result in a lower precision SC estimate (SC = 0.92). The five oxide

Moiti Tuff

SC (low-Fe) = 0.92;
SC (High-Fe) = 0.95

(3.89±0.02, $^{39/40}$Ar; White et al., 1993)
(3.92±0.04, $^{39/40}$Ar; White et al., 1994)

△ Arabian Sea; 722A 12-4 (90-120 cm)
○ Gulf of Aden; 231-22-1 (82 cm)
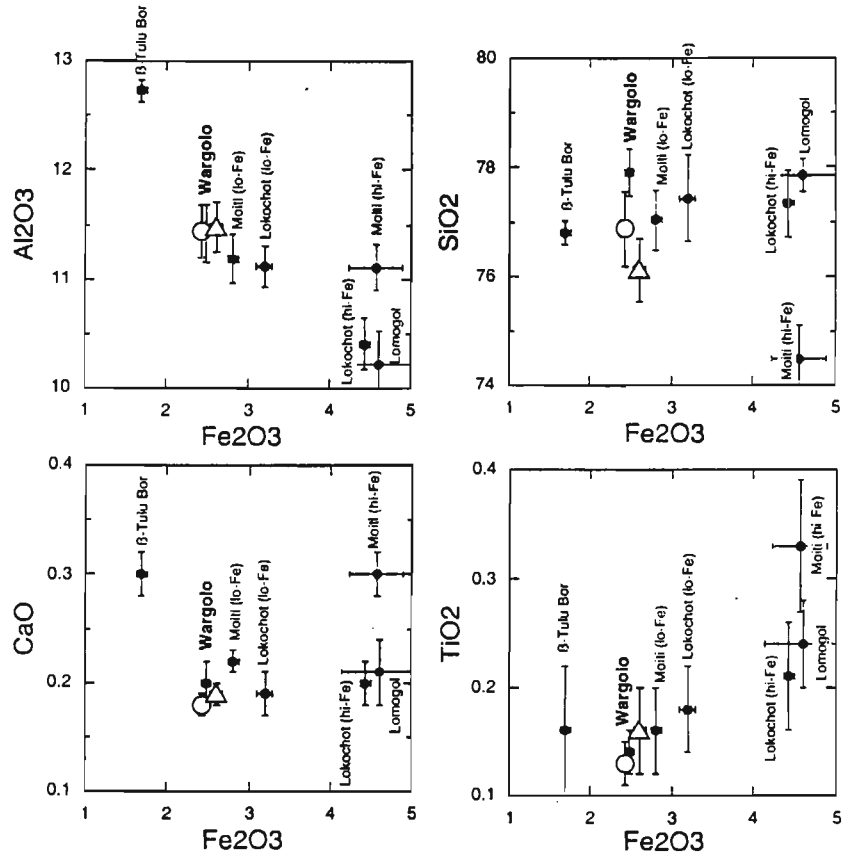● Kenya/Ethiopia tuff chemistries

[Figure 3.6]
Crossplots of major element oxide percentage compositions for high-Fe and low-Fe endmembers of Moiti Tuff volcanic glass shards from the Turkana Basin, Kenya (closed circles), Gulf of Aden (open circles), and the Arabian Sea (open triangles). All data were recalculated to 100% on a fluid-free basis (Tables 3.2–3.4); error bars represent one standard deviation.

40

Wargolo

SC=0.95

(Age: 3.80±0.05 Ma, Haileab and Brown, 1994, interp. from Cindery Tuff)

△ Arabian Sea - 721C 13-3 (90-120 cm)
○ Gulf of Aden - 231-21-2 (33-34)
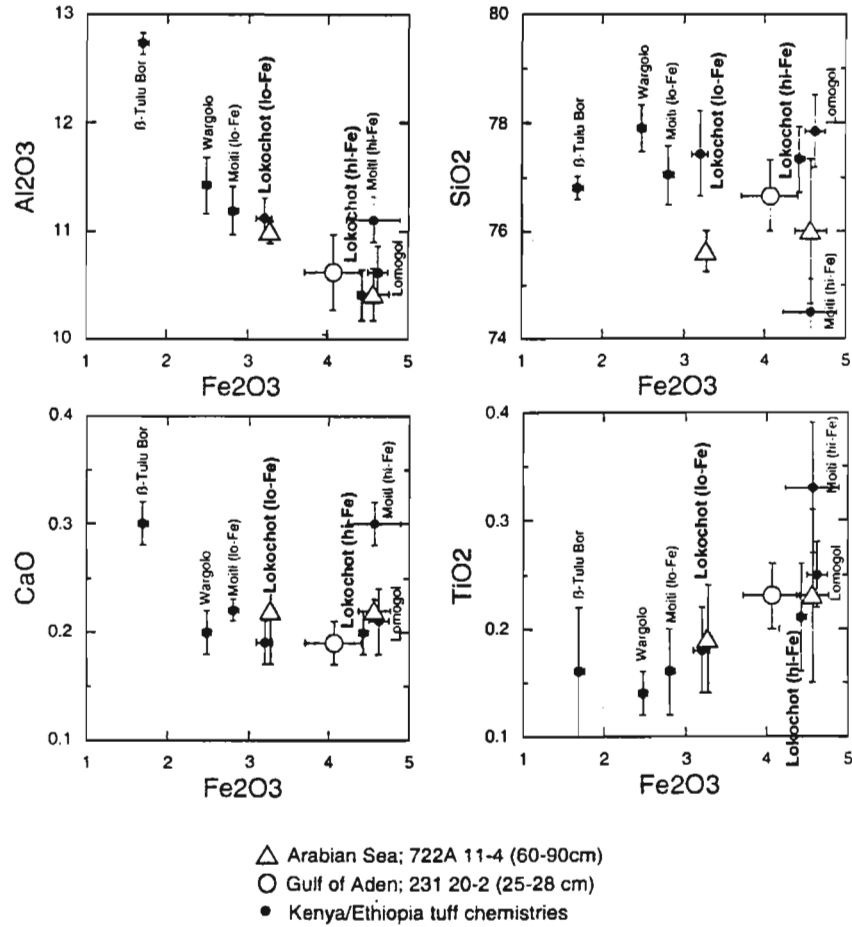● Kenya/Ethiopia tuff chemistries

[Figure 3.7]
Crossplots of major element oxide percentage compositions for Wargolo Tuff volcanic glass shards from the Turkana Basin, Kenya (closed circles), Gulf of Aden (open circles), and the Arabian Sea (open triangles). All data were recalculated to 100% on a fluid-free basis (Tables 3.2–3.4); error bars represent one standard deviation.

Lomogol

SC=0.98

(Age: ~3.7 Ma; interpolation between Lokochot and Moiti)

△ Arabian Sea; 722A 11-5 (60-90cm)
○ Gulf of Aden; 232A 1-5 (25-27 cm)
● Kenya/Ethiopia tuff chemistries
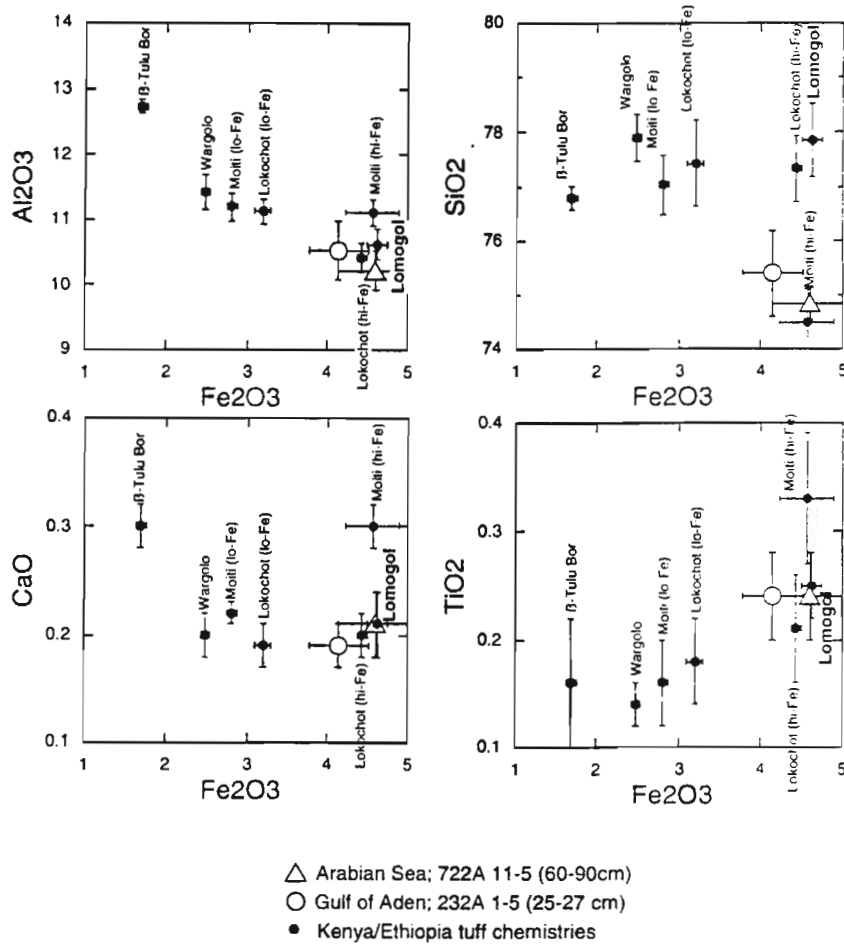
[Figure 3.8]
Crossplots of major element oxide percentage compositions for Lomogol Tuff volcanic glass
shards from the Turkana Basin, Kenya (closed circles), Gulf of Aden (open circles), and the
Arabian Sea (open triangles). All data were recalculated to 100% on a fluid-free basis (Tables
3.2–3.4); error bars represent one standard deviation.

Lokochot

SC (low-Fe) = 0.95
SC (Hi-Fe) = 0.95

(Age: ~3.58-3.60 Ma, at Mat./Gauss reversal)

△ Arabian Sea; 722A 11-4 (60-90cm)
○ Gulf of Aden; 231 20-2 (25-28 cm)
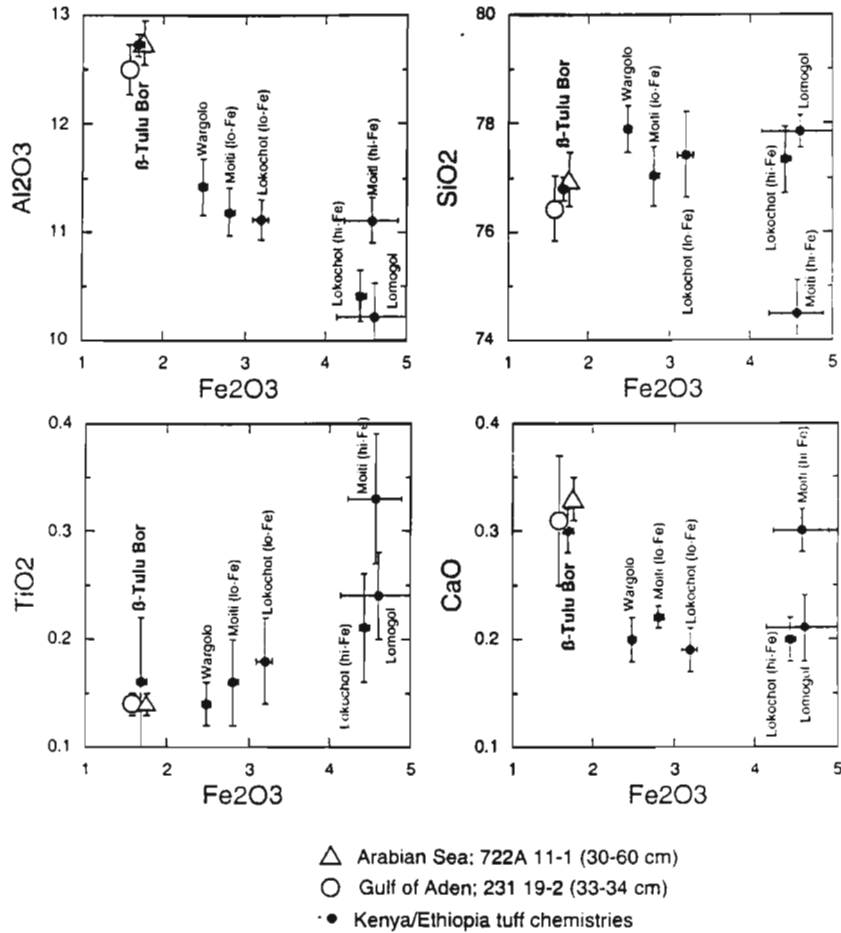● Kenya/Ethiopia tuff chemistries

[Figure 3.9]
Crossplots of major element oxide percentage compositions for high-Fe and low-Fe
endmembers of Lokochot Tuff volcanic glass shards from the Turkana Basin, Kenya (closed
circles), Gulf of Aden (open circles), and the Arabian Sea (open triangles). All data were
recalculated to 100% on a fluid-free basis (Tables 3.2–3.4); error bars represent one standard
deviation.

β -Tulu Bor

(SC=0.95)

(Age: 3.39±0.04, SHT $^{39/40}$Ar; White et al., 1993)

43

△ Arabian Sea: 722A 11-1 (30-60 cm)
○ Gulf of Aden: 231 19-2 (33-34 cm)
● Kenya/Ethiopia tuff chemistries

[Figure 3.10]
Crossplots of major element oxide percentage compositions for β-Tulu Bor Tuff volcanic glass shards from the Turkana Basin, Kenya (closed circles), Gulf of Aden (open circles), and the Arabian Sea (open triangles). All data were recalculated to 100% on a fluid-free basis (Tables 3.2–3.4); error bars represent one standard deviation.

44

compositions for sample 722A 12-4 (90–120 cm) match those for the low-Fe (K81-602) and high-Fe (83-1 ANU) Moiti compositions within one-sigma analytical variability (Fig. 3.6). Additionally, the low-Fe Moiti composition was also identified within the Gulf of Aden samples at Site 231 (Sample 231 22-1 (82 cm); Sarna-Wojcicki *et al.*, 1985). The Gulf of Aden oxide compositions are also plotted on Fig. 3.6, closely matching (SC = 0.94; Table 3.5) those from the Arabian Sea. The orbitally tuned age for the Moiti Tuff in the Arabian Sea sequence is 3.96 ± 0.01 Ma (Fig. 3.5, Table 3.6).

Sample 721C 13-3 (90–120 cm) – Wargolo Tuff (SC = 0.95)

The oxide plots for this sample are shown compared to the East African tuff compositions in Fig. 3.7. This sample is distinguished by its intermediate Fe, Si, and Al oxide composition and lower Ca and Ti oxide percentages. Based on an average of six shard analyses this sample most closely matches (SC = 0.95; Tables 3.2–3.5) the Wargolo Tuff (K81-485; Tables 3.2–3.4). The Wargolo Tuff was also identified within the Gulf of Aden sediments (231 21-2 (33–34 cm) and its oxide composition also closely matches (SC = 0.92; Table 3.5) the Arabian Sea data (Fig. 3.7). The Wargolo Tuff oxide compositions are readily distinguished from the stratigraphically underlying (older) Cindery Tuff (3.85 ± 0.08 Ma; White, 1993) which has characteristically much higher Al_2O_3, TiO_2, CaO percentages relative to the Wargolo composition (Brown *et al.*, 1992; Haileab & Brown, 1992). The orbitally tuned age for the Wargolo Tuff in the Arabian Sea sequence is 3.80 ± 0.01 Ma (Fig. 3.5, Table 3.6).

Sample 722A 11-5 (60–90 cm) – Lomogol Tuff (SC = 0.98)

Average oxide compositions for twenty shards from the Arabian Sea sample 722A 11-5 (60–90 cm) are shown compared to the East African Tuff compositions in Fig. 3.8. The best compositional match for this sample is with the Lomogol Tuff (SC = 0.98, K82-742; Tables 3.2–3.4), as evidenced by its distinctive high-Fe and low Ca and Al oxide composition (Table 3.5, Fig. 3.8). The Gulf of Aden oxide data shown in Fig. 3.8 have been correlated to the Lomogol Tuff (Brown *et al.*, 1992; Sarna-Wojcicki *et al.*, 1985). This composition closely matches the Arabian Sea Lomogol-equivalent (SC = 0.95; Tables 3.2–3.5). The Arabian Sea and Gulf of Aden SiO_2 data are lower than those for the Turkana Basin sample K82-742 but it should be noted that SiO_2 data for this and other tuffs can be highly variable between samples due, in part, to higher relative percentage error and significant intersample SiO_2 variability. The Lomogol oxide composition is very close to the high-Fe Lokochot composition which commonly confounds efforts to distinguish between

Table 3.6. *Comparison of orbitally tuned and radiometric ages of East African tuffs between 3.4 Ma and 4.0 Ma*

Tuff	721/722 Orbitally tuned Age (Ma)	Kenyan/Ethiopian sites Radiometric Age (Ma)	Reference
β-Tulu Bor/SHT	3.41 ± 0.01 Ma	3.39 ± 0.04 Ma	(White, 1993)
		3.41 ± 0.01 Ma	(Walter and Aronson, 1993)
Wargolo/VT-1	3.80 ± 0.01 Ma	3.80 ± 0.05 Ma	(Haileab and Brown, 1992)
		3.75 ± 0.02 Ma	(White, 1993)
Moiti/VT-3	3.96 ± 0.01 Ma	≤ 4.10 ± 0.07 Ma	(McDougall, 1985)
		3.89 ± 0.02 Ma	(White, 1993)
		3.94 ± 0.04 Ma	(White et al., 1994)

these two compositionally similar tuffs. However, the younger Lokochot Tuff has a characteristic bimodal high-Fe and low-Fe composition which, when both compositions are present in a single sample, can be used diagnostically (see below). The orbitally tuned age for the Lomogol Tuff in the Arabian Sea sequence is 3.62 ± 0.01 Ma (Fig. 36).

Sample 722A 11-4 (60–90 cm) – Lokochot Tuff (SC = 0.95)

The oxide compositions for Arabian Sea sample 722A 11-4 (60–90 cm) are shown compared to the East African tuff compositions in Fig. 3.9. Oxide analyses from this sample identified separate low-Fe and high-Fe endmember compositions (Fig. 3.9, Table 3.2) These two compositions closely match the oxide compositions for the high-Fe (SC = 0.95, $n = 6$) and low-Fe (SC = 0.95, $n = 14$) compositions of the Lokochot Tuff (Fig. 3.9, Tables 3.2–3.5). As noted above, the high-Fe Lokochot is compositionally similar to the Lomogol Tuff, but we correlate these Arabian Sea tephra to the Lokochot Tuff because of the dual high-Fe and low-Fe compositions and its proper stratigraphic position above (younger than) the Lomogol Tuff (Brown et al., 1992; Haileab & Brown, 1992). The Gulf of Aden data for the high-Fe end member of the Lokochot Tuff (sample 231 20-2 (25–28 cm)) also match the Arabian Sea oxide data (SC = 0.94; Fig. 3.9, Table 3.5). The orbitally tuned age for the Lokochot Tuff in the Arabian Sea sequence is 3.57 ± 0.01 Ma (Fig. 3.5, Table 3.6).

Sample 722A 11-1 (30–60 cm) – β-Tulu Bor Tuff (SC = 0.95)

The oxide compositions for Arabian Sea sample 722A 11-1 (30–60 cm) are shown compared to the East Africa tuff compositions in Fig. 3.10. Although

Radioisotopic & Stratigraphic Ages

Orbitally-tuned Ages
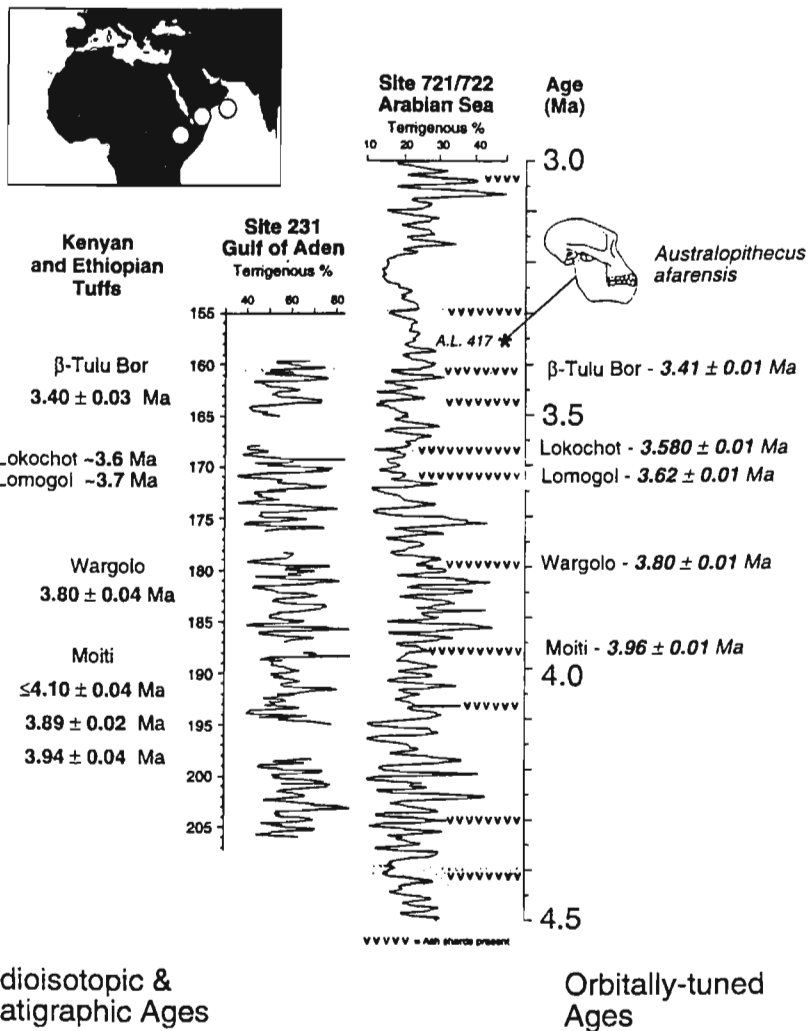
[Figure 3.11]

Comparison of radiometric and stratigraphic (interpolated) ages for East African tuffs between 4.0–3.4 Ma and their orbitally tuned ages derived from the marine sediment chronostratigraphy at Sites 721 and 722 in the Arabian Sea. Tephra correlations between East Africa, the Gulf of Aden, and the Arabian Sea sediments were accomplished using major element oxide compositions (Figs. 3.6–3.10; Tables 3.2–3.5). Note that the radiometric and orbitally tuned ages agree to within their joint error, or generally within 0.01 Ma. New, orbitally tuned ages can be applied to the Lokochot and Lomogol Tuffs for which direct radiometric age determinations have not yet been possible. Placement of the fossil hominid cranium A.L. 417 (*Australopithecus afarensis*) within the context of the eolian dust record at Site 721/722 was constrained by its stratigraphic position relative to the Sidi Hakoma Tuff (SHT, = β-Tulu Bor).

we were only able to analyse a single shard from this level (Table 3.2), its composition was sufficiently diagnostic (very low Fe and Ti, high Al and Ca oxide values) to make a tentative correlation to the β-Tulu Bor Tuff (SC = 0.95; Table 3.5). This is the only East African tuff within this time interval that has such a composition. The β-Tulu Bor Tuff was also detected in the Gulf of Aden sediments (Sample 231 19-2 (33–34 cm)) and those oxide data are shown in Fig. 3.10 (Sarna-Wojcicki *et al.*, 1985). The Gulf of Aden data from sample 231 19-2 (33–34 cm) also match the Arabian Sea oxide data (SC = 0.96; Table 3.5). The orbitally tuned age for the β-Tulu Bor Tuff in the Arabian Sea sequence is 3.41 ± 0.01 Ma (Fig. 3.5, Table 3.6).

Discussion

Tephrostratigraphic links between East Africa, the Gulf of Aden, and the Arabian Sea

Despite very low volcanic shard abundances in these Arabian Sea samples we have been able to extract, concentrate, and analyse them by electron microprobe and establish oxide correlations to known East African tuffs. For each of the five tephra presented in Figs. 3.6–3.10 the geochemical data were sufficiently diagnostic to establish firm correlations to specific East African tuff compositions with Similarity Coefficient values ranging between 0.92 and 0.98. Additionally, we used the Squared Chord Distance parameter (D^2) as defined by Perkins *et al.* (1995) as a more quantitative means to evaluate the oxide similarity between an analysed tephra and other candidate match tephras. The advantage of this D^2 parameter is that it employs the mean oxide data as well as their associated analytical standard deviations to assign statistical significance levels to a proposed tephra correlation, since D^2 has a Chi-square distribution among compositionally identical samples (Perkins *et al.*, 1995, 1998). Calculating this chord distance parameter for our analyses we found that the β-Tulu Bor Tuff correlation was significant at the 99% level, the Moiti Lokochot Tuff correlations were significant at the 95% level, and the Wargolo and Lomogol Tuff correlations were significant between the 90% and 95% confidence levels.

Using these tephrostratigraphic correlations we can now compare directly the radiometric ages obtained from land tephra to the orbitally tuned ages of correlative tephra preserved in the marine sediments. Additionally, we can use the correlations to assign new, orbitally tuned ages to those tuffs which have not been radiometrically dated and are only presently constrained by stratigraphic age interpolations.

Comparison of radioisotopic and orbitally tuned tephra ages

The eolian dust record at Sites 721/722 is constrained by an orbitally tuned chronostratigraphy with an approximate tuning precision of ±5 kyr (see deMenocal, 1995) The absolute error of the chronology may deviate from sideral time by up to 5–15 kyr due to remaining uncertainties of the phase of this record with respect to orbital forcing (Clemens *et al.*, 1996). The nominal temporal resolution of the tephra extraction samples from Sites 721/722 was 10 kyr. Thus, we adopt a nominal joint tuning and sampling error of ±0.01 Ma for the orbitally tuned ages presented in the following discussion.

The Moiti Tuff – 722A 12-4 (90–120 cm)

We obtain an orbitally tuned age of 3.96 ± 0.01 Ma for the Moiti tephra identified within sample 722A 12-4 (90–120 cm) (Figs. 3.3–3.5 and Fig. 3.11). Tephra shards were found at high concentrations over a 60 cm interval (119.00–119.60 mcd), spanning 3.95–3.98 Ma. Feldspar grains within the Moiti tuff from the Turkana Basin, northern Kenya were initially K–Ar dated with a maximum age of ≤ 4.10 ± 0.07 Ma (McDougall, 1985). Subsequent $^{40}Ar/^{39}Ar$ laser-fusion dating of single crystals within the VT-1 Tuff from Aramis, Ethiopia (= Moiti) has refined this estimate to 3.89 ± 0.02 Ma (White, 1993) and 3.94 ± 0.04 Ma (White *et al.*, 1994). Eight published dates for the VT-1 Tuff in White (1993) ranged between 3.786 and 4.065 Ma with a single (unweighted) standard deviation of 0.08 Ma about the 3.89 Ma mean value (see Table 1 in White *et al.*, 1993).

The Wargolo Tuff – 721C 13-3 (90–120 cm)

We obtain an orbitally tuned age of 3.80 ± 0.01 Ma for the Wargolo tephra identified within sample 721C 13-3 (90–120 cm) (Figs. 3.3–3.5, Fig. 3.11). Shards were found at high concentrations between 114.45–115.05 mcd, spanning 3.79–3.81 Ma. This age also agrees extremely well with the co-occurrence of the extinction of the coccolithophorid *Reticulofenestra pseudoumbilica* at this same level within these sediments, also dated at 3.80 ± 0.04 Ma (Tiedemann *et al.*, 1994). Haileab & Brown (1992) estimated the age of the Wargolo Tuff at 3.80 ± 0.05 Ma based on stratigraphic interpolation between adjacent well-dated tuffs. Single crystal sanidine $^{40}Ar/^{39}Ar$ dates on the VT-3 Tuff (= Wargolo) from Aramis, Ethiopia yielded an age of 3.75 ± 0.02 Ma for this horizon (White, 1993). Published dates (13 analyses) on VT-3 Tuff (= Wargolo) ranged between 3.65 and 3.89 Ma, with a single (unweighted) standard deviation of 0.09 Ma about the 3.75 Ma mean value (see Table 1 in White, 1993).

β-Tulu Bor Tuff – 722A 11-1 (30–60 cm)

We obtain an orbitally tuned age of 3.41 ± 0.01 Ma for the β-Tulu Bor tephra identified within sample 722A 11-1 (30–60 cm) (Figs. 3.3–3.5, Fig. 3.11). Shards were found in high concentrations over a broader 90 cm interval (102.15–102.45 mcd), spanning 3.40–3.43 Ma, with a well defined peak at 102.30 mcd (3.41 Ma). The β-Tulu Bor Tuff correlates between many localities on land and the deep sea (Brown, 1982; Brown & Cerling, 1982; Brown *et al.*, 1992; Sarna-Wojcicki *et al.*, 1985), and has been the focus of many dating efforts (Haileab & Brown, 1992, 1994; McDougall, 1985; McDougall *et al.*, 1992; Walter & Aronson, 1993; White, 1993). The Sidi Hakoma Tuff of the Hadar Formation (Middle Awash) is compositionally similar and temporally equivalent to the β-Tulu Bor Tuff of the Koobi Fora Formation (Turkana Basin), Tuff B of the Shungura Formation and Tuff U-10 of the Usno Formation of southwestern Ethiopia, and a tuff in the Kipcherere section of the Chemeron Formation in the Baringo Basin of Kenya (Brown, 1982; Walter & Aronson, 1993; Namwamba, 1993), suggesting that it is the product of a very broadly dispersed airfall tephra from a large volcanic eruption, most likely near Munesa at the eastern rim of the Main Ethiopian Rift (Walter & Aronson, 1993). Single crystal laser-fusion $^{40}Ar/^{39}Ar$ dates on ten (rare) feldspars from the Sidi Hakoma Tuff document an age of 3.406 ± 0.007 Ma for this eruption (Walter & Aronson, 1993). Also using single crystal, laser-fusion analysis, White (1993) dated the Sidi Hakoma Tuff at 3.39 ± 0.04 Ma. Both of these radioisotopic dates for the β-Tulu Bor Tuff agree well with our orbitally tuned age of 3.41 ± 0.01 Ma.

Assignment of orbitally tuned ages to previously undated tephra

We can assign orbitally tuned ages to the Lokochot and Lomogol Tuffs for which direct radioisotopic dates have not been obtainable. Ages for these tuffs have been estimated based on stratigraphic interpolation between adjacent, radioisotopically dated horizons and paleomagnetic polarity stratigraphy.

Lokochot Tuff – 722A 11-4 (60–90 cm)

The orbitally tuned age of the Lokochot Tuff for sample 722A 11-4 (60–90 cm) is 3.58 ± 0.01 Ma (Fig. 3.11, Table 3.7). Vitric shards occur in elevated abundances over a 60 cm interval associated with this horizon (107.25–107.85 mcd) which spans 3.56–3.58 Ma; peak abundances occur at the analysed level (107.70 mcd; 3.58 Ma). The age of the Lokochot Tuff was

Table 3.7. *Comparison of orbitally tuned ages and stratigraphically interpolated ages of East African tuffs between 3.4 Ma and 4.0 Ma*

Tuff	721/722 Orbitally tuned Age (Ma)	Kenyan/Ethiopian/ marine sediment Stratigraphic Age (Ma)	Reference
Lokochot Tuff	3.58 ± 0.01 Ma	~ 3.50–3.60 Ma	(Sarna-Wojcicki *et al.*, 1985)
		~ 3.50 Ma	(Haileab and Brown, 1992)
		3.58 Ma	(Hilgen, 1991)
		3.57 Ma	(McDougall *et al.*, 1992)
		3.59 ± 0.03 Ma	(Tiedemann *et al.*, 1994)
		3.59 Ma	(Shackleton *et al.*, 1990)
Lomogol Tuff	3.62 ± 0.01 Ma	~ 3.6 Ma	(Haileab and Brown, 1992)
		3.6 ± 0.1 Ma	(Pickford *et al.*, 1991)

estimated at ~ 3.5–3.6 Ma based on its stratigraphic placement within Site 231 from the Gulf of Aden (Sarna-Wojcicki *et al.*, 1985). Within the Kenyan and Ethiopian sequences the Lokochot Tuff occurs almost precisely at the Gauss/Gilbert paleomagnetic reversal (Feibel *et al.*, 1989; Hillhouse *et al.*, 1986) which is presently dated by orbital tuning of various independent stratigraphic sequences at 3.59 ± 0.03 Ma (Tiedemann *et al.*, 1994), 3.59 Ma (Shackleton *et al.*, 1990, 1994), and 3.58 Ma (Hilgen, 1991), and 3.57 Ma by stratigraphic interpolation between adjacent radioisotopically dated tuffs from the Turkana Basin (McDougall *et al.*, 1992).

Lomogol Tuff – 722A 11-5 (60–90 cm)

The orbitally tuned age of the Lomogol Tuff within sample 722A 11-5 (60–90 cm) is 3.62 ± 0.10 Ma (Fig. 3.11, Table 3.7). Vitric shards that occur are abundant over a 60 cm interval associated with this horizon (108.75–109.35 mcd) which spans 3.61–3.63 Ma. The Lomogol Tuff is known from the north end of the Labur Range in the Turkana Basin of north Kenya (K82-742). It has also been detected in the Western Rift Valley of Uganda (Pickford *et al.*, 1991) and in the Gulf of Aden marine sequences (Brown *et al.*, 1992). In the Turkana Basin the age of Lomogol Tuff was estimated to be ~ 3.6 Ma because it lies stratigraphically between the Lokochot and the Moiti Tuffs (Feibel *et al.*, 1989; Haileab & Brown, 1992).

Conclusions

Ages of hominid and other vertebrate fossils from East African Pliocene-Pleistocene sedimentary sequences are largely constrained by direct

radiometric dating and regional intercorrelation of numerous volcanic tuff beds. Several of these tuff beds have been directly dated using K/Ar and ^{40}Ar/^{39}Ar methods but many tuffs have not yet been dated or have insufficient juvenile feldspar grain concentrations for analysis. The detection and analysis of tephra within adjacent marine sediments (Brown *et al.*, 1992; Sarna-Wojcicki *et al.*, 1985) presents a new opportunity to date a majority of tephra within the context of the very detailed and precise orbitally tuned marine sediment chronostratigraphy (Hilgen, 1991; Shackleton *et al.*, 1990, 1994; Tiedemann *et al.*, 1994). Here we have focused on the mid-Pliocene (3.4–4.0 Ma) record of tephra deposition and associated oxide chemistry within marine sediments from the Arabian Sea, some 2000 km distant from East African source volcanoes.

Despite very low vitric shard abundances within the Arabian Sea sediments, sufficient shards were separated from the layers with the most abundant shards for electron microprobe analysis. Major element oxide compositions were used to establish firm geochemical correlations to five known Turkana Basin tuffs between 3.4–4.0 Ma and their correlative tephra in the Gulf of Aden (β-Tulu Bor, Lokochot, Lomogol, Wargolo, and Moiti Tuffs).

As the Arabian Sea sequence is temporally constrained by an orbitally tuned chronostratigraphy we can use these tephrostratigraphic correlations to directly compare the East African K/Ar and ^{40}Ar/^{39}Ar radiometric ages with the marine orbitally tuned ages. Radioisotopic and orbitally tuned ages generally agree within ±0.01 Ma for each of the three mid-Pliocene tuffs where both age determinations were available (β-Tulu Bor, Wargolo, Moiti Tuffs). We have assigned new (orbitally tuned) ages to the Lokochot and Lomogol Tuffs for which direct radiometric dates were not available.

We present this as a proof-of-concept study. We estimate that a total of 25–30 separate tephra horizons can be similarly analysed, intercorrelated, and dated for the Pliocene–Pleistocene (0.5–4.5 Ma) interval at Sites 721 and 722 in the Arabian Sea. Once complete, these terrestrial–marine tephra correlations will provide a framework for direct testing of hypotheses linking known changes in African hominid and other vertebrate evolution to known changes in regional (African) and global climate.

References

Behrensmeyer, A. K., Todd, N. E., Potts, R. & McBrinn, G. E. 1997. Late Pliocene faunal turnover in the Turkana Basin, Kenya and Ethiopia. *Science*, **278**, 1589–94.

Berger, A. & Loutre, M. F. 1991. Insolation values for the climate of the last 10 million years. *Quat. Sci. Reviews*, **10**, 297–317.

52

Bloemendal, J. & deMenocal, P. B. 1989. Evidence for a change in the periodicity of tropical climate cycles at 2.4 Myr from whole-core magnetic susceptibility measurements. *Nature*, **342**, 897–9.

Borchardt, G. A., Aruscavage, P. J. & Millard, H. T. 1972. Correlation of the Bishop Ash, a Pleistocene marker bed, using instrumental neutron activation analysis. *J. Sed. Petrol.*, **42** (2), 301–6.

Brown, F. H. 1982. Tulu Bor tuff at Koobi Fora correlated to the Sidi Hakoma Tuff at Hadar. *Nature*, **300**, 631–5.

Brown, F. H. & Cerling, T. E. 1982. Stratigraphic significance of the Tulu Bor Tuff. *Nature*, **299**, 212–15.

Brown, F. H., Sarna-Wojcicki, A. M., Meyer, C. E. & Haileab, B. 1992. Correlation of Pliocene and Pleistocene tephra layers between the Turkana Basin of East Africa and the Gulf of Aden. *Quaternary International*, **13/14**, 55–67.

Clemens, S. C., Murray, D. W. & Prell, W. L. 1996. Nonstationary phase of the Plio-Pleistocene Asian Monsoon. *Science*, **274**, 943–8.

Clemens, S. C. & Prell, W. L. 1990. Late Pleistocene variability of Arabian Sea summer monsoon winds and continental aridity: Eolian records from the lithogenic component of deep-sea sediments. *Paleoceanography*, **5**, 109–45.

Clemens, S. & Prell, W. L. 1991. One million year record of summer monsoon winds and continental aridity from the Owen Ridge (Site 722), Northwest Arabian Sea. In *Preceedings of the Ocean Drill. Prog.*, Prell, W. J. & Niitsuma, N. (eds.), pp. 365–88. Ocean Drill. Proj., College Station, TX.

Clemens, S., Prell, W., Murray, D., Shimmield, G. & Weedon, G. 1991. Forcing mechanisms of the Indian Ocean monsoon. *Nature*, **353**, 720–5.

deMenocal, P. B. 1995. Plio-Pleistocene African Climate. *Science*, **270**, 53–9.

deMenocal, P. B. & Bloemendal, J. 1995. Plio-Pleistocene subtropical African climate variability and the paleoenvironment of hominid evolution: A combined data-model approach. In *Paleoclimate and Evolution With Emphasis on Human Origins*, Vrba, E., Denton, G., Burckle, L. & Partridge, T. (eds.), pp. 262–88. Yale University Press, New Haven.

deMenocal, P. B., Bloemendal, J. & King, J. W. 1991. A rock-magnetic record of monsoonal dust deposition to the Arabian Sea: Evidence for a shift in the mode of deposition at 2.4 Ma. In *Proc. Ocean Drill. Prog., Scientific Results*, Prell, W. L., Niitsuma, N. *et al.* (eds.), pp. 389–407. Ocean Drilling Program, College Station, TX.

deMenocal, P. B. & Rind, D. 1993. Sensitivity of Asian and African climate to variations in seasonal insolation, glacial ice cover, sea-surface temperature, and Asian orography. *J. Geophys. Res.*, **98** (4), 7265–87.

deMenocal, P. B., Ruddiman, W. F. & Pokras, E. M. 1993. Influences of high- and low-latitude processes on African climate: Pleistocene eolian records from equatorial Atlantic Ocean Drilling Program Site 663. *Paleoceano.*, **8** (2), 209–42.

Feibel, C. S., Brown, F. H. & McDougall, I. 1989. Stratigraphic context of fossil hominids from the Omo Group Deposits: Northern Turkana Basin, Kenya. *Amer. J. Phys. Anthro.*, **78**, 595–622.

Grine, F.E. 1986. Ecological causality and the pattern of Plio-Pleistocene hominid evolution in Africa. *S. Afr. J. Sci.*, **82**, 87–9.

Haileab, B. & Brown, F. H. 1992. Turkana Basin-Middle Awash Valley correlations and the age of the Sagantole and Hadar Formations. *J. Hum. Evol.*, **22**, 453–68.

Haileab, B. & Brown, F. H. 1994. Tephra correlation between the Gadeb prehistoric site

and the Turkana Basin. *J. Hum. Evol.*, **26**, 167–73.

Hastenrath, S. 1985. *Climate and Circulation of the Tropics*. D. Reidel. Boston.

Hilgen, F. J. 1991. Astronomical calibration of Gauss to Matuyama sapropels in the Mediterranean and implication for the geomagnetic polarity timescale. *Earth and Planet. Sci. Lett.*, **104**, 226–44.

Hillhouse, J. W., Cerling, T. E. & Brown, F. H. 1986. Magnetostratigraphy of the Koobi Fora Formation, Lake Turkana, Kenya. *J. Geophys. Res.*, **91** (B11), 11581–95.

Kutzbach, J.E. 1981. Monsoon climate of the early Holocene: Climatic experiment with the earth's orbital parameters for 9000 years ago. *Science*, **214**, 59–61.

Kutzbach, J.E. & Guetter, P. J. 1986. The influence of changing orbital parameters and surface boundary conditions on climate simulations for the past 18,000 years. *J. Atmos. Sci.*, **43**, 1726–59.

McDougall, I. 1985. K-Ar and 40Ar-39Ar dating of the hominid-bearing Pliocene-Pleistocene sequence at Koobi Fora, Lake Turkana, northern Kenya. *Geol. Soc., Amer. Bull.*, **96**, 159–75.

McDougall, I., Brown, F. H., Cerling, T. E. & Hillhouse, J. W. 1992. A reappraisal of the geomagnetic polarity timescale to 4 Ma using data from the Turkana Basin, East Africa. *Geophys. Res. Lett.*, **19** (23), 2349–52.

Murray, D. W. & Prell, W. L. 1991. Pliocene to Pleistocene variations in calcium carbonate, organic carbon, and opal on the Owen Ridge, Northern Arabian Sea. In *Proc. O.D.P., Sci. Res.*, Prell, W. L. & Niitsuma, N. (eds.), pp. 343–55. Ocean Drilling Program, College Station. TX.

Nair, R. R., Ittekot, V., Manganini, S., Ramaswamy, V., Haake, B., Degens, E., Desai, B. & Honjo, S. 1989. Increased particle flux to the deep ocean related to monsoons. *Nature*, **338**, 749–51.

Namwamba, F. 1993. Tephrostratigraphy of the Chemeron Formation. Baringo Basin, Kenya, M.S. thesis, University of Utah, Salt Lake City.

Nash, W. P. 1992. Analysis of oxygen with the electron microprobe: applications to hydrated glass and minerals, *Amer. Min.*, **77**, 453–7.

Perkins, M. E., Brown, F. H., Nash, W. P., McIntosh, W. & Williams. S. K. 1998. Sequence, age, and source of silicic fallout tuffs in middle to late Miocene basins of the northern Basin and Range province. *Geol. Soc. Amer. Bull.*, 110 (3), 344–60.

Perkins, M. E., Nash, W. P., Brown, F. H. & Fleck, R. J. 1995. Fallout tuffs of Trapper Creek, Idaho – A record of Miocene explosive volcanism in the Snake River Plain volcanic province. *Geol. Soc. Amer. Bull.*, **107**, 1484–506.

Pickford, M., Senut, B., Poupeau, G., Brown, F. H. and Haileab, B. 1991. Correlation of tephra layers from the Western Rift Valley (Uganda) to the Turkana Basin (Ethiopean/Kenya) and the Gulf of Aden. *C. R. Acad. Sci. Paris*, 313 (II), 223–9.

Pouchou, J.-L. & Pichoir, F. 1991. Quantitative analysis of homogeneous or stratified microvolumes applying the model 'PAP'. In *Electron Probe Quantitation*. Heinrich, K. F. J. & Newbury, D. E. (eds.), pp. 31–75. Plenum Press, New York.

Prell, W. L. & Kutzbach, J. E. 1987. Monsoon variability over the past 150,000 years. *J. Geophys. Res.*, **92**, 8411–25.

Prell, W. L. & Kutzbach, J. E. 1992. Sensitivity of the Indian monsoon to forcing parameters and implications for its evolution. *Nature*, **360**, 647–52.

Prell, W. L. & Niitsuma, N. 1988. Milankovitch and monsoons. *Nature*. **331**, 663–4.

Prell, W. L., Niitsuma, N. & Emeis, K. 1988. Leg 117 finds mountains, monsoons. *Geotimes*, **33** (3), 13–16.

Pye, 1987. *Eolian Dust and Dust Deposits*, Academic Press, New York.

54   Renne, P., Walter, R., Verosub, K., Sweitzer, M. & Aronson, J. 1993. New data from Hadar (Ethiopia) support orbitally-tuned time scale to 3.3 Ma. *Geophys. Res. Lett.*, **20** (11), 1067–70.

Sarna-Wojcicki, A. M. & Davis, J. O. 1991. Quaternary tephrochronology. In *Quaternary Nonglacial Geology, Conterminous U.S.*, R. B. Morrison (ed.), pp. 93–116. Geol. Soc. Amer., Geol. N. Amer., Boulder, CO.

Sarna-Wojcicki, A. M., Meyer, C. E., Roth, P. H. & Brown. F. H. 1985. Ages of tuff beds at East African early hominid sites and sediments in the Gulf of Aden. *Nature*, **313**, 306–8.

Shackleton, N. J., Berger, A. & Peltier, W. R. 1990. An alternative astronomical calibration of the lower Pleistocene timescale based on ODP Site 677. *Transactions of the Royal Society of Edinburgh: Earth Sciences*, **81**, 251–61.

Shackleton, N. J., Crowhurst, S., Hagelberg, R., Pisias, N. J. & Schneider, D. A. 1994. A new late Neogene time scale: Application to leg 138 sites. In *Scientific Results, ODP Leg 138*, Mayer, L., Pisias, N. J. & Janecek, T. (eds.). Ocean Drilling Program, College Station, TX.

Sirocko, F. 1989. Accumulation of eolian sediments in the northern Indian Ocean: record of the climatic history of Arabia and India. *Berichte-Reports, Geol.-Paläont. Inst. Univ. Kiel*, **27**, 1–114.

Sirocko, F., Garbe-Schonberg. D., McIntyre, A. & Molfino, B. 1996. Teleconnections between the subtropical monsoons and high-latitude climates during the last deglaciation. *Science*, **272**, 526–9.

Sirocko, F. & Sarnthein, M. 1989. Wind-borne deposits in the northwestern Indian Ocean: record of Holocene sediments versus modern satellite data. In *Paleoclimatology and Paleometeorology: Modern and Past Patterns of Global Atmospheric Transport*, Leinen, M. & Sarnthein, M. (eds.), pp. 401–33. Kluwer Academic Publishers.

Tiedemann, R., Sarnthein, M. & Shackleton, N. J. 1994. Astronomic timescale for the Pliocene Atlantic d18O and dust flux records of ODP Site 659. *Paleoceanography*, **9** (4), 619–38.

Vrba, E. 1995. The fossil record of African antelopes (Mammalia, Bovidae) in relation to human evolution and paleoclimate. In *Paleoclimate and Evolution With Emphasis on Human Origins*, Vrba, E., Denton, G., Burckle, L. & Partridge, T. (eds.), pp. 385–424. Yale University Press, New Haven.

Vrba, E. S. 1985. Ecological and adaptive changes associated with early hominid evolution, in *Ancestors: The Hard Evidence*, E. Delson (ed.), pp. 63–71. A. R. Liss, New York, NY.

Walter, R. C. 1994. Age of Lucy and the First Family: Single-crystal 40/39 Ar dating of the Denen Dora and lower Kada Hadar members of the Hadar Formation, Ethiopia. *Geology*, **22**, 6–10.

Walter, R. C. & Aronson, J. L. 1993. Age and source of the Sidi Hakoma Tuff, Hadar Formation, Ethiopia. *J. Hum. Evol.*, **25**, 229–40.

White, T. D. 1993. New discoveries of *Australopithecus* at Maka in Ethiopia. *Nature*, **366**, 261–5.

White, T. D., Suwa, G. & Asfaw, B. 1994. *Australopithecus ramidus*, a new species of early hominid from Aramis, Ethiopia. *Nature*, **371**, 306–12.

WoldeGabriel, G., White, T, D., Suwa, G., Renne, P., deHeinzelin, J., Hart, W. K. & Heiken, G. 1994. Ecological and temporal placement of early Pliocene hominids at Aramis, Ethiopia. *Nature*, **371**, 330–3.